

Xinqiao Zhang, Tamsin O'Reilly, Kristina Holsgrove, John Scott, Iaroslav Gaponenko, Praveen Kumar, Joshua Agar, Patrycja Paruch, Miryam Arredondo

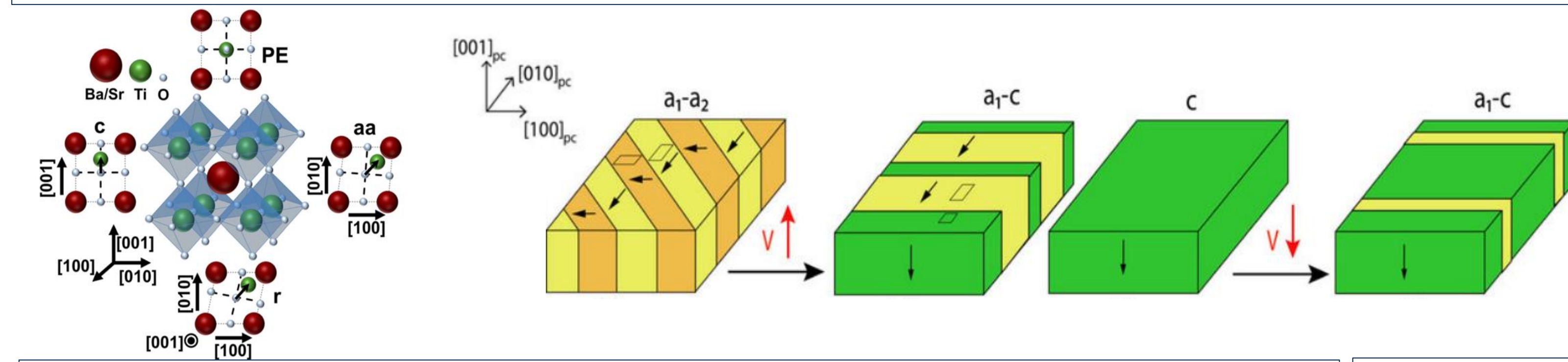
Introduction

Ferroelectrics exhibit spontaneous polarization and reversible switching, playing a crucial role in applications like non-volatile FeRAM, ferro-TFET, and catalysis. However, understanding the influence of environmental factors on ferroelectric domain dynamics is challenging due to limited in-situ observation. This study investigates the impact of temperature and background gas on domain mapping of Barium Titanate (BTO), focusing on in-plane $\langle 110 \rangle$ (a-a), and mixed in/out-of-plane $\langle 100 \rangle$ (a-c) polarized domains.

Deep learning techniques address data challenges caused by sample warping and reduced signal-to-noise ratio. Prior research conducted by the M3L group has employed autoencoders to learn domain structures from Scanning Transmission Electron Microscopy (STEM) images, and used affine transforms to learn symmetry. In this study, we enhance the approach by simulating diffraction patterns using windowing and Fourier Transforms (FFT), which are commonly utilized in electron microscopy. An autoencoder with rotation, translation, and scaling affine grids learns symmetries and periodicities of FFT windows, creating a condensed representation of the original data.

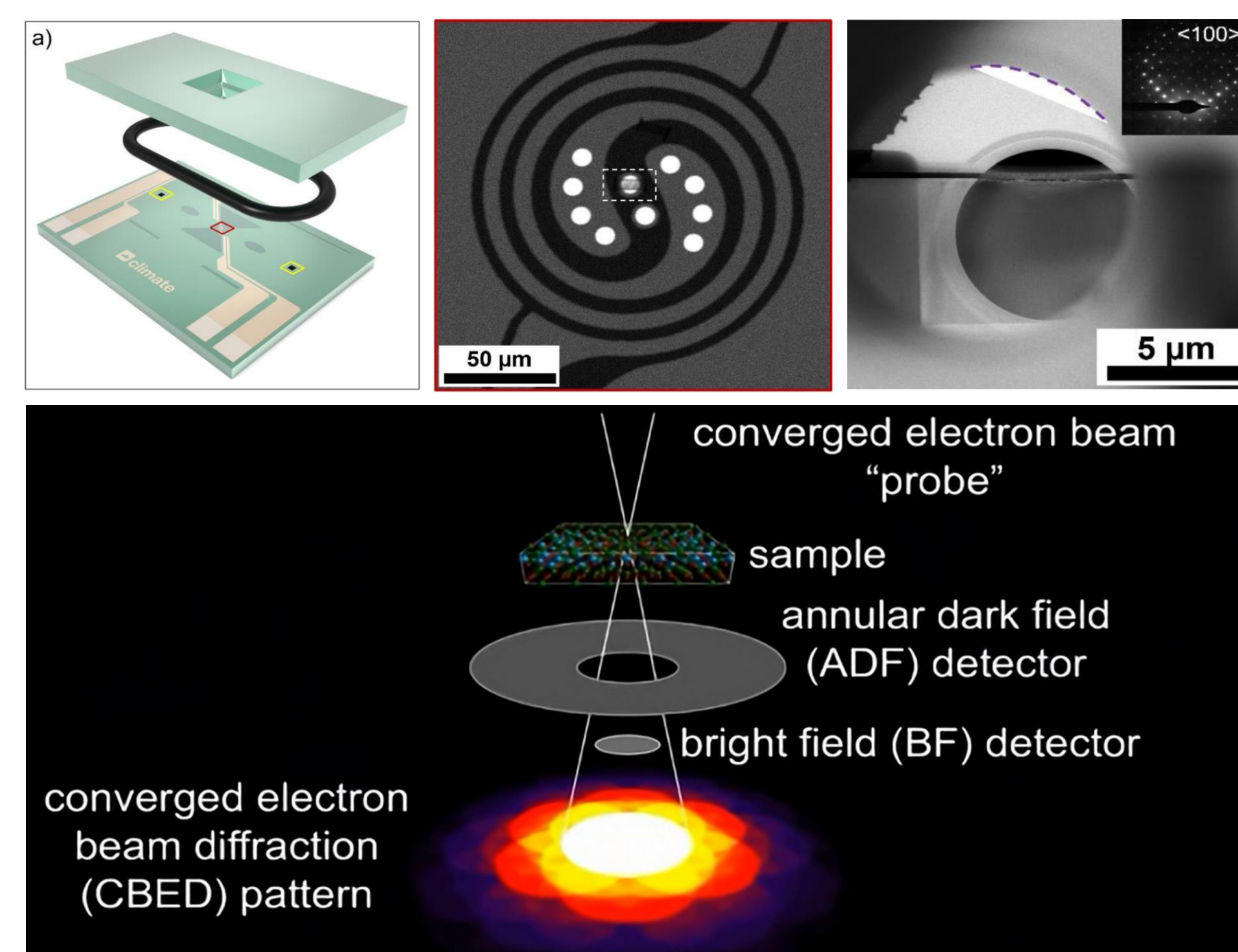
The methodology characterizes phases, sample warping, and contamination in BTO samples across three environments: Ultra High Vacuum (UHV), 20% Nitrogen/Argon, and 20% Oxygen/Argon. The UHV experiment provides the best signal-to-noise ratio, establishing phases and warping in the embedding. Transfer learning allows applying the pre-trained weights to further training in Nitrogen, Oxygen, and Annealed UHV samples.

Symmetry-informed autoencoders offer efficient analysis compared to manual phase mapping, removing human bias and enabling real-time analysis of brightfield images. Transfer learning enables training on accessible ferroelectric materials like BTO and applies the knowledge to novel ferroelectrics with similar structures, even those requiring custom growth.



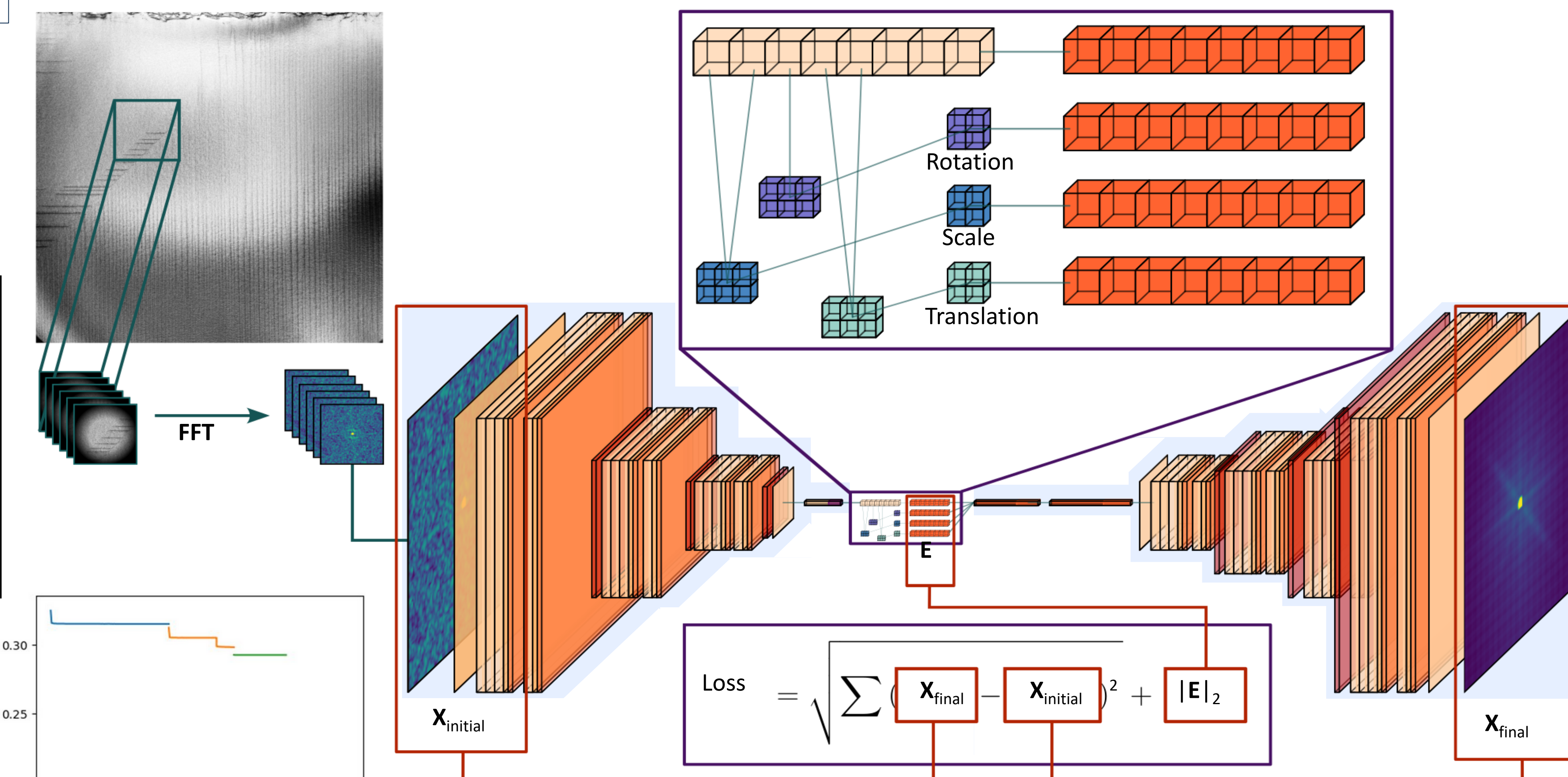
Experimental Setup

- BTO samples were milled to ~ 150 nm using Gallium Focused Ion Beam (FIB), and in-situ heating and gas control were achieved with the DENSSolution Climate System.
- The heating cycle consisted ran from Room Temperature $\rightarrow 250^\circ\text{C} \rightarrow$ Room Temperature, capturing High Angle Annular Dark Field (HAADF) and Bright Field STEM (BF-STEM) images every 5°C .
- Background gases for Oxygen and Nitrogen were mixed with Argon (inert gas) at a 20% ratio. The pressure and flow rate were set at 900 mbar and 0.3 ml/min, respectively. Prior to the start of the experiment, the chamber was flushed for 5 minutes.



Model Setup

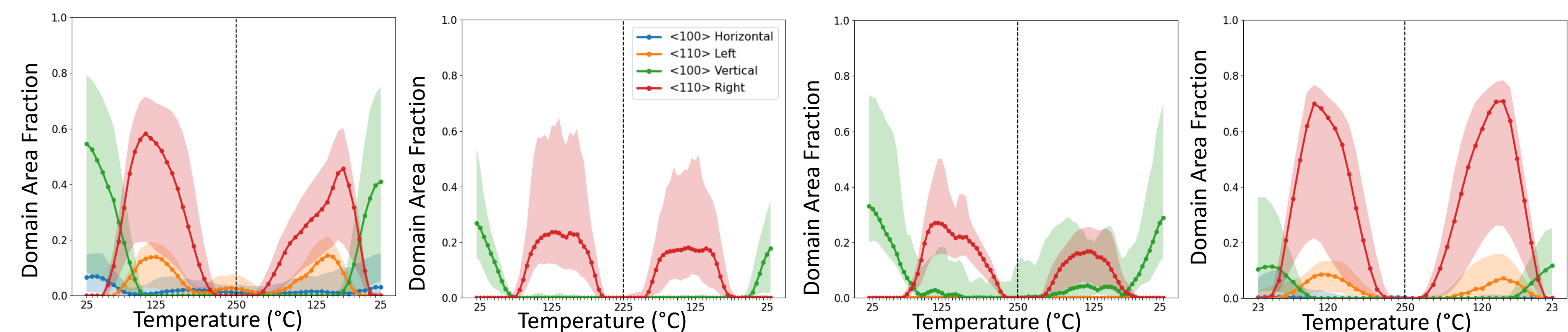
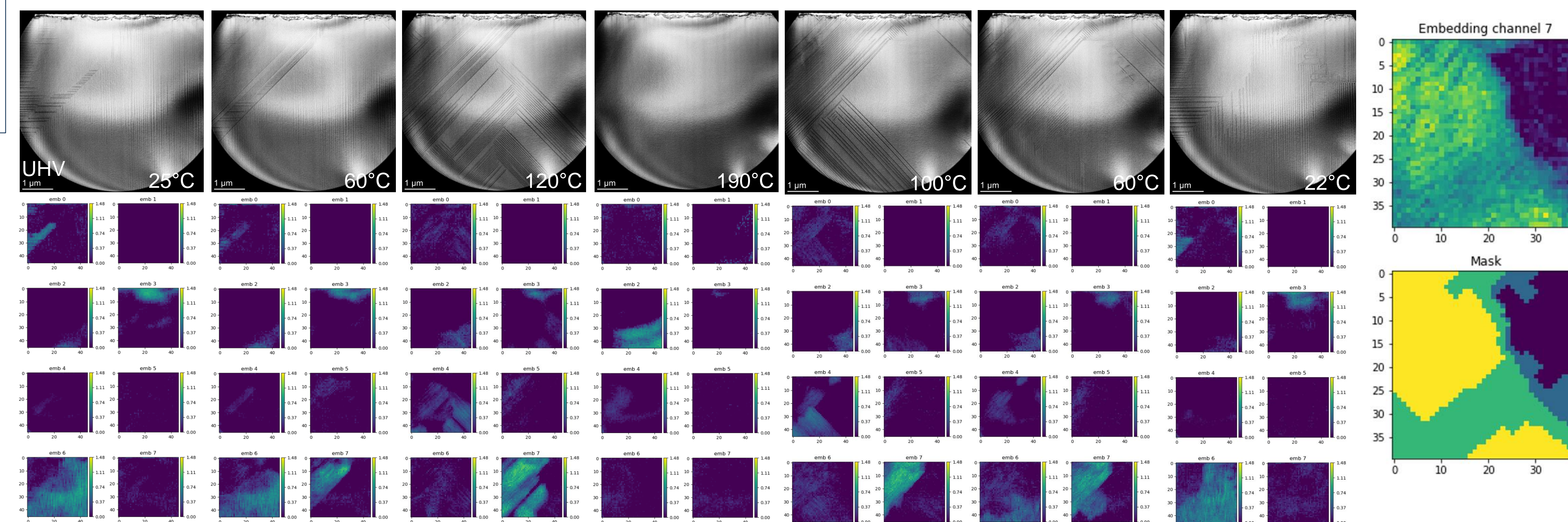
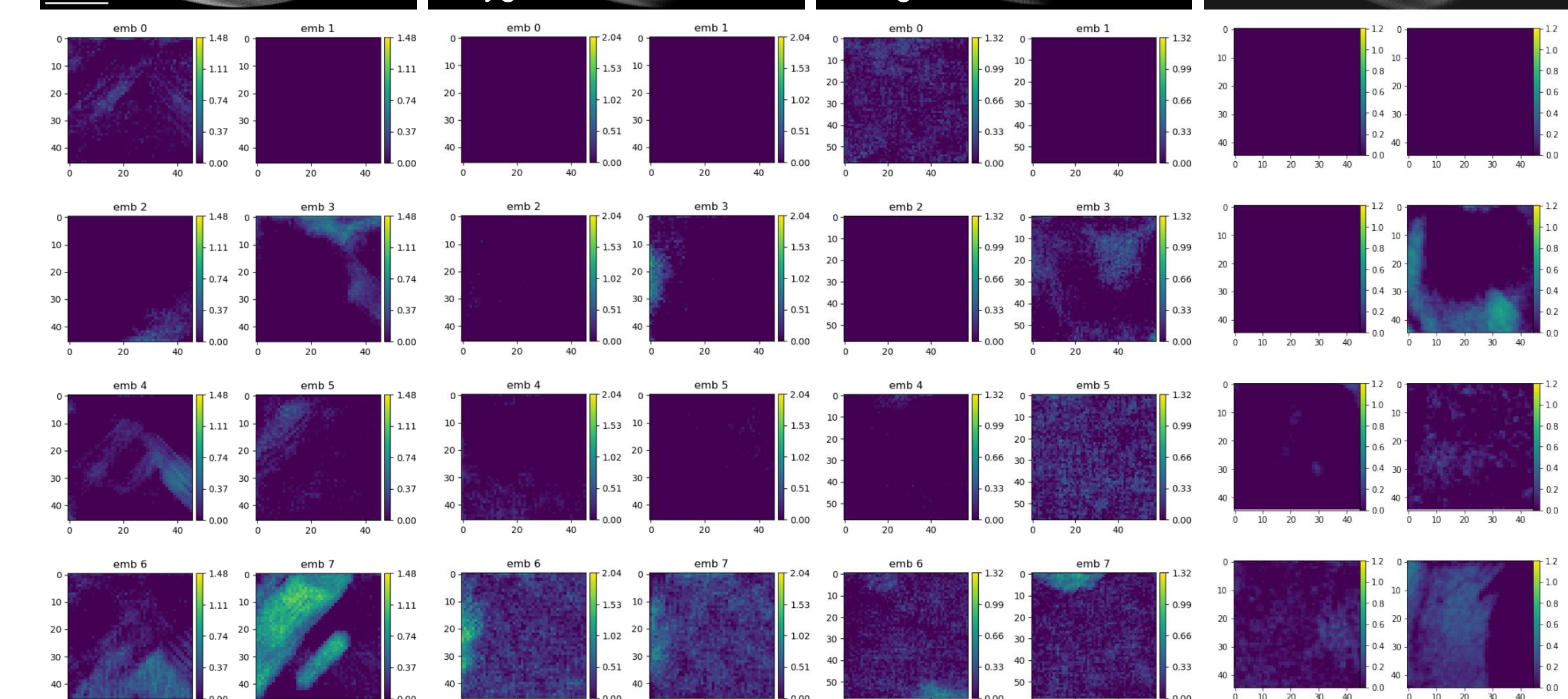
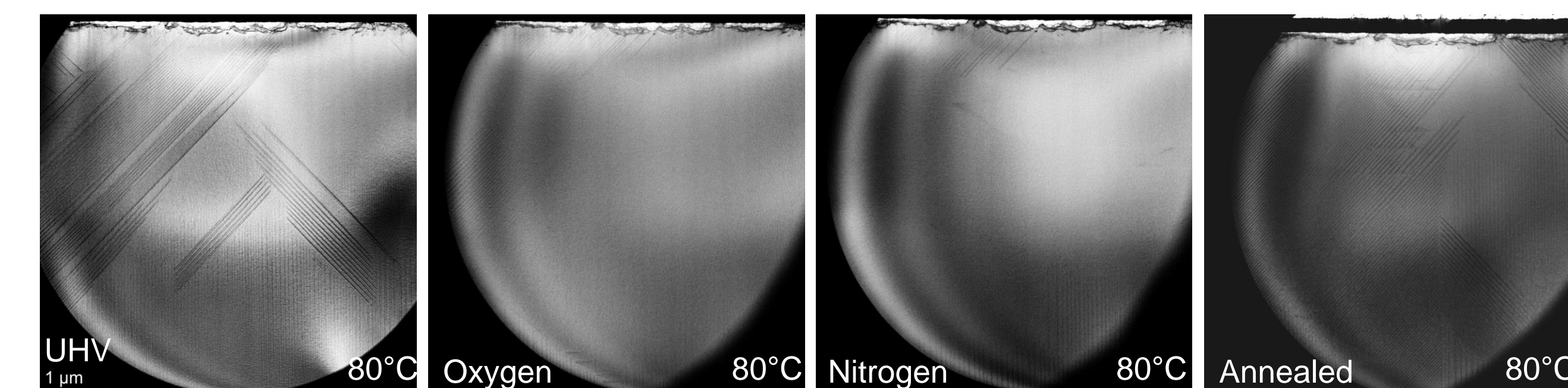
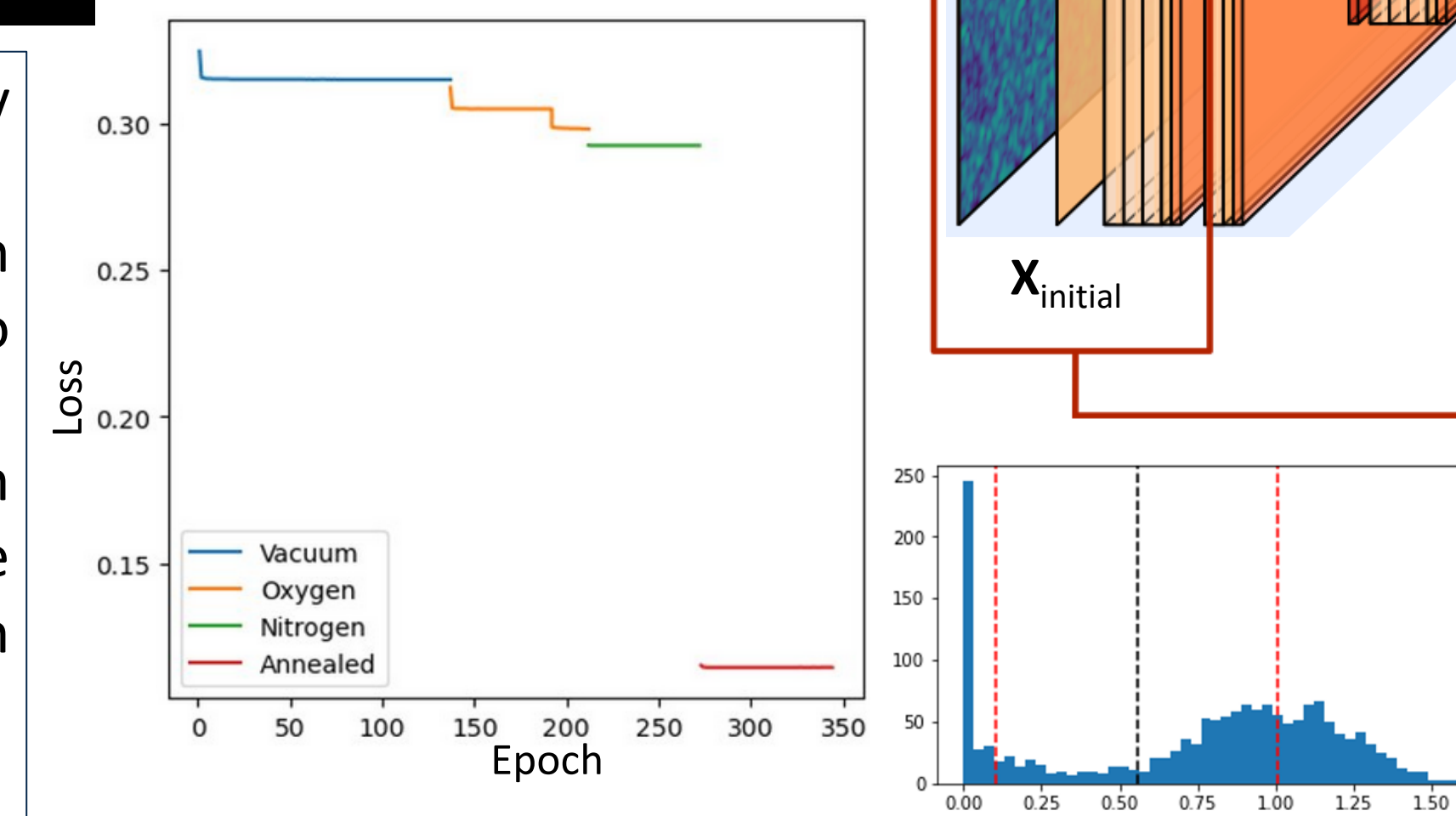
- Preprocessing includes cropping, gaussian filtering, sampling size (128,128) sliding windows with step size of 32. Then a hanning window, FFT, logarithm, and standard scaling are applied to the windows.
- The input dataset contains $T \times N \times N$ images, where N represents the number of windows taken in the x and y direction. The model is inspired by the Joint Rotationally Invariant Variational Autoencoder.
- The Encoder utilizes 2D convolutional layers and ReLU activation function to downsample the input data into an 8-point feature vector. Each block includes 20% dropout to prevent overfitting. The first 5 terms of the feature vector represent x-scaling, y-scaling, x-translation, y-translation, and rotation in radians. These terms are used to construct rotational, scaling, and translational affine matrices, which are then used to generate 2×2 affine grids.
- The grids are flattened and appended to the feature vector. The Decoder uses this augmented feature vector to reconstruct the original input.
- The loss function is the mean squared error (MSE) between the original and reconstructed data. Additionally, an L1 penalty is added to the final embedding vector to encourage sparsity and prevent overfitting.



Results

- Model distinguished embedding channels [0,4,6,7] as horizontal a-c, left slanted a-a, vertical a-c, and right slanted a-a domains in Vacuum. Additionally, channel 2 corresponded to sample warping.
- Oxygen and Nitrogen environments had lower SNR ratio, but the model was able to train with steadily decreasing loss and generate robust results in less epochs when trained with transferred weights from previous training.
- Segmentation in the pressure environments was not as clear as in Vacuum. The model often confused channels 4, and 6 with the right slanted a-a domain and 3 with left slanted. The model also confused channel 4 with contamination in of Oxygen environment.
- The Annealed sample also had less clear segmentation due to problems during STEM scan which resulted in less data available.

- UHV: Dense $\langle 100 \rangle$ a-c domains form until 60°C , then are replaced by $\langle 110 \rangle$ a-a domains. Domains disappear around 190°C .
- Nitrogen: Domain wall formation is suppressed in both inert Nitrogen and reactive Oxygen environment, there was less coexistence of the two phases, and higher Curie temperature.
- Oxygen: There is mottling due to contamination from either gallium oxide, which formed due to gallium implantation during milling on the FIB, or a separate TiO or BaO species which formed in an oxygen rich environment.
- Annealed UHV: Similar trends to UHV environment.



Conclusions

- The UHV environment facilitated the formation of dense metastable competing a-c and a-a domains.
- Conversely, the presence of Oxygen and Nitrogen suppressed domain formation, with Oxygen exhibiting distinct surface reactions.
- The pinning of domain walls by oxygen vacancies explains the heightened prominence of domains in UHV environments.
- By employing windowing and frequency domain transformations, we successfully segmented images and distinguished false signals.
- Additionally, the integration of affine grids greatly enhanced the deep learning model's capacity to learn symmetry and periodicity.



Award No. 2215789
Award No. 2246463

Acknowledgements



References

- Buck, D. A. (1952). In *Ferroelectrics for digital information storage and switching*. Ft. Belvoir, Defense Technical Information Center.
- Ding, W., Lu, J., Tang, X., Kou, L., & Liu, L. (2023). Ferroelectric materials and their applications in activation of small molecules. *ACS Omega*, 8(7), 6164–6174. <https://doi.org/10.1021/acsomega.2c06828>
- Kalinin, S. V., Mukherjee, D., Roccapriore, K. M., Blaiszik, B., Ghosh, A., Ziatdinov, M. A., Al-Najjar, A., Doty, C., Akers, S., Rao, N. S., Agar, J. C., & Spurgeon, S. R. (2023, April 4). Deep learning for automated experimentation in scanning transmission electron microscopy. *2304.02048*
- Nguyen, T. N., Guo, Y., Qin, S., Frew, K. S., Xu, R., & Agar, J. C. (2021). Symmetry-aware recursive image similarity exploration for materials microscopy. *Npj Computational Materials*, 7(1). <https://doi.org/10.1038/s41524-021-00637-y>
- Zhu, Z., Persson, A. E., & Wernersson, L.-E. (2023). Reconfigurable signal modulation in a ferroelectric tunnel field-effect transistor. *Nature Communications*, 14(1). <https://doi.org/10.1038/s41467-023-38242-w>